Deletion of Seventeen Amino Acids at the C-Terminal End of Aquaporin 0 Causes Distortion Aberration and Cataract in the Lenses of AQP0$^{\Delta C/\Delta C}$ Mice

Kulandaiappan Varadaraj and Sindhu Kumari

Department of Physiology and Biophysics, Renaissance School of Medicine, Stony Brook University, Stony Brook, New York, United States

Correspondence: Kulandaiappan Varadaraj, Department of Physiology and Biophysics, Renaissance School of Medicine, Stony Brook University, Stony Brook, NY 11794-8661, USA; kulandaiappan.varadaraj@stonybrook.edu.

Submitted: December 9, 2018
Accepted: January 21, 2019

Citation: Varadaraj K, Kumari S. Deletion of seventeen amino acids at the c-terminal end of aquaporin 0 causes distortion aberration and cataract in the lenses of AQP0$^{\Delta C/\Delta C}$ mice. *Invest Ophthalmol Vis Sci*. 2019;60:858–867. https://doi.org/10.1167/iovs.18-26378

Purpose. Investigate the effects of the absence of 17 amino acids at the C-terminal end of Aquaporin 0 (AQP0) on lens transparency, focusing property, and homeostasis.

Methods. A knockin (KI) mouse model (AQP0$^{\Delta C/\Delta C}$) was developed to express AQP0 only as the end-cleaved form in the lens. For this, AQP0 was genetically engineered as C-terminally end-cleaved with amino acids 1 to 246, instead of the full length 1 to 263 of the wild type (WT). After verifying the KI integration into the genome and its expression, the mouse model was bred for several generations. AQP0 KI homozygous (AQP0$^{\Delta C/\Delta C}$) and heterozygous (AQP0$^{+/\Delta C}$) lenses were imaged and analyzed at different developmental stages for transparency. Correspondingly, aberrations in the lens were characterized using the standard metal grid focusing method. Data were compared with age-matched WT, AQP0 knockout (AQP0$^{-/-}$), and AQP0 heterozygous (AQP0$^{+/-}$) lenses.

Results. AQP0$^{\Delta C/\Delta C}$ lenses were transparent throughout the embryonic development and until postnatal day 15 (P15) in contrast to age-matched AQP0$^{-/-}$ lenses, which developed cataract at embryonic stage itself. However, there was distortion aberration in AQP0$^{\Delta C/\Delta C}$ lens at P5; after P15, cataract began to develop and progressed faster surpassing that of age-matched AQP0$^{-/-}$ lenses. AQP0$^{+/\Delta C}$ lenses were transparent even at the age of 1 year in contrast to AQP0$^{+/-}$ lenses; however, there was distortion aberration starting at P15.

Conclusions. A specific distribution profile of intact and end-cleaved AQP0 from the outer cortex to the inner nucleus is required in the lens for establishing refractive index gradient to enable proper focusing without aberrations and for maintaining transparency.

Keywords: AQP0, lens transparency, spherical aberration, cataractogenesis, C-terminal cleaved AQP0

The ocular lens needs to be transparent for proper vision. Structurally, the lens has a monolayer of epithelial cells at the anterior surface, beneath which lie multiple layers of fiber cells. The epithelial cells at the equator transform and differentiate into the secondary fiber cells. It is a continuous process. Because there is no cellular turnover, all the fiber cells produced in a life span are contained within the lens. As new fiber cells are added over the older differentiating fiber cells in the outer cortex, inner cortical, and outer nuclear fiber cells undergo maturation and compaction for which loss of cellular nuclei, organelles, cytoskeletal proteins as well as reduction in the extracellular space and water becomes essential. These processes help to organize the fiber cells in a precise manner to minimize light scattering. The oldest fiber cells occupy the center of the ellipsoidal crystalline lens, which grows peripherally. Constant addition of the fiber cells increases the bulk and could lead to spherical aberration (SA), which creates multiple focal points and blurred vision. To circumvent this, the lens adjusts the refractive index gradient (RING),[1,2] which varies from 1.386 to 1.406 from the cortex to the nucleus in humans[3,4] and 1.35 to 1.55[5] in mouse. RING adjustment is a cooperative process mediated by several proteins and post-translational modifications.

Aquaporin (AQP) water channels are integral membrane proteins belonging to the superfamily of Aquaporins. They are expressed in microbes, plants, and animals and are critical for cellular development, growth, and homeostasis. AQPs allow transcellular passage of water (aquaporins) or water and small solutes like glycerol (aquaglyceroporins). Water channels, gap junction channels, ion transporters, and cotransporters are involved in creating a microcirculation within the lens to compensate for its avascular nature by providing the necessary nutrients and removing the metabolic wastes.[6–8]

In mammals, 13 different AQP genes have been identified. The mammalian lens expresses AQP0, AQP1, and AQP5. Mammalian AQP0 is a 28-kDa protein that is profusely expressed in the lens contributing approximately 45% of the total membrane proteins of the fiber cells.[9] It is a multifunctional protein. Water permeability[10–14] and cell-to-cell adhesion (CTCA)[15–20] functions of AQP0 are important for maintaining lens transparency,[12,15,16,21] refractive index gradient,[2,22] biomechanics,[23] and homeostasis.[6–8,24] AQP0 displays a characteristically low water permeability,[11,12,14] which is several-fold less compared with its lens counterparts AQP1 and AQP5. Mutations and knockout of AQP0 alter ocular growth and result in dominant cataracts due to the loss of lens homeostasis,

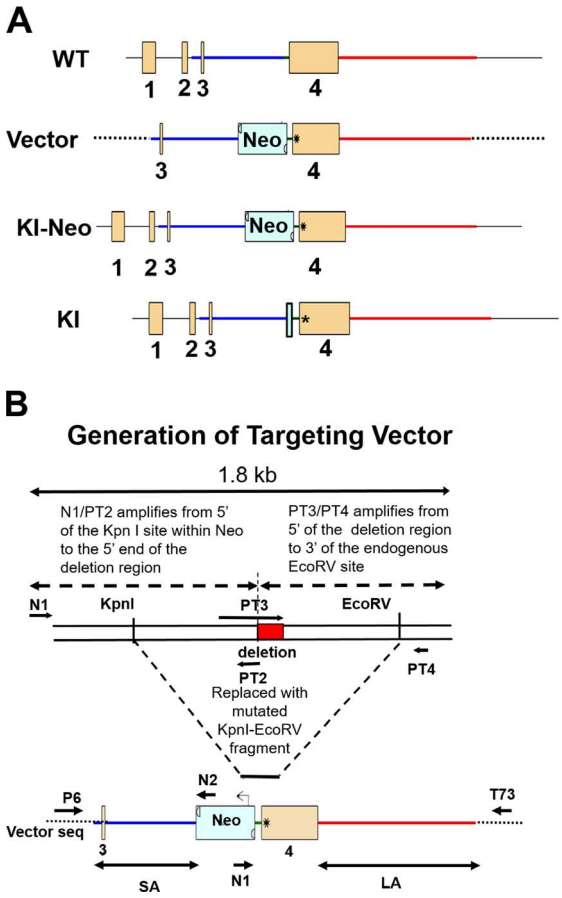

Figure 1. Strategy to generate a AQP0$^{\Delta C/\Delta C}$ by introducing a stop codon after amino acid 246. (**A**) WT: Schematic structure of WT mouse *AQP0* gene showing exons 1-4 (as *rectangular vertical* or *horizontal boxes*) and the connecting introns. Vector: Exons 3 and 4 with introns (highlighted in *blue* and *red*) as well as a Neo selection gene were amplified by PCR and cloned into the vector (details in [**B**]). *Black dotted lines* on either side denote vector sequences. *Asterisk* indicates an in-frame translation stop codon predicted to truncate AQP0 after the amino acid Asparagine-246. KI-Neo: The recombinant vector (with Exons 3 and 4, introns highlighted in *blue* and *red* and the Neo selection gene) was transfected into mouse embryonic stem cells and positive clones were selected using the Neo selection marker. KI: KI with stop codon after amino acid 246 but without the Neo-Selection marker. *Light green vertical rectangle* indicates one set of the LoxP-FRT sites that remain after Neo deletion (74 bp). Positive embryonic stem cells selected were injected into mouse blastocysts to develop AQP0 KI mouse model (AQP0$^{\Delta C/\Delta C}$). (**B**) Schematic of the introduction of the stop codon through a point mutation incorporated into a primer pair (to delete the 17 amino acids after the 246th), and the KI targeting vector design. The C-terminal end deletion was engineered by overlap extension PCR using the primers as indicated. *Red rectangle* represents the deletion region. SA, short homology arm; LA, long homology arm. N1, N2, PT2, PT3, PT4, P6, and T73 are forward or reverse primers used, as indicated.

whereas, knockout of AQP1[25] or AQP5[26] does not cause cataract under normal conditions. The cataract phenotype due to alteration in AQP0, highlights the importance of the unique functions of this protein for lenticular homeostasis.[2,16,23,27–34]

Protein hydropathy and crystallography analyses envisage six transmembrane domains and cytoplasmic N- and C-terminal domains for the AQP superfamily. In AQP0, the C-terminus modulates water permeability[35,36]; it binds to cytoskeletal proteins to ensure proper fiber cell alignment.[37–40] Several posttranslational modifications (PTMs), such as phosphorylation, deamidation, and isomerization occur at this domain.[40] A particularly important PTM is N- and/or C-terminal end-truncation, which begins at the inner cortex of the lens. Presence of truncated forms increases as the fiber cells age. Higher concentrations of such forms were noticed in the nuclear region of the lens than in the cortex. Presence of cleaved forms of AQP0[22,41–45] crystallin,[46,47] connexins (Cx50[48–51] and Cx46[52,53]), and beaded filament proteins[54,55] in the fiber cells does not affect lens transparency. N-terminal end-cleavage sites, which remove 2 to 6 and 2 to 12 amino acids of AQP0 in the normal lens have been reported.[42,45,56,57] C-terminal end-cleavage sites at residues 228, 234, 239, 243, 245, 246, 247, 249, and 259 in human AQP0 have been identified using mass spectrometry.[43,45]

Among the three AQPs expressed in the lens, only AQP0 undergoes gradient loss of N- and C-terminal ends.[43,45,57] The cleavage of N- and C-terminal ends of AQP0 has long been considered as a consequence of the onset of senescence. However, this type of PTM occurs as early as 2 years after birth in the human lens.[41] There is a dearth of investigations aimed at understanding the significance of the presence of intact and cleaved forms of AQP0, connexins, and crystallins in gradients in the lens. We developed an AQP0 knockin (KI) mouse model (AQP0$^{\Delta C/\Delta C}$) by engineering the *AQP0* gene to express a predominant posttranslationally C-terminal end-cleaved form having amino acids 1 to 246. This mouse model was further investigated to understand the necessity for the presence of intact AQP0 (1–263 amino acids) with reference to lens optical quality and focusing. Our results clearly demonstrate that absence of intact AQP0 in the lens causes distortion aberration and cataract.

Materials and Methods

Animals

The wild type (WT) and mouse models used in this investigation are in C57BL/6J (The Jackson Laboratory, Bar Harbor, ME, USA) inbred strain which does not carry the *CP49* gene mutation. WT (AQP0$^{+/+}$), AQP0 heterozygous (AQP0$^{+/-}$), AQP0 knockout (AQP0$^{-/-}$), and a newly developed C-terminally end-deleted AQP0 mutant KI in homozygous (AQP0$^{\Delta C/\Delta C}$) and heterozygous (AQP0$^{+/\Delta C}$) genotypes were used. WT mouse in FVB strain was used as a positive control for *CP49* mutation. For animal procedures, the ARVO Statement for the Use of Animals in Ophthalmic and Vision Research, the National Institutes of Health's (NIH; Bethesda, MD, USA) "Guide for the Care and Use of Laboratory Animals" and protocols approved by Stony Brook University Animal Care and Use Committee were followed.

Generation of AQP0-1-246 Mutant Knockin (AQP0$^{\Delta C/\Delta C}$) Mouse Model

A truncated mutant AQP0 KI mouse model AQP0$^{\Delta C/\Delta C}$ was developed through inGenious Targeting Laboratory, Inc. (Ronkonkoma, NY, USA). This model expresses a major form of C-terminally end-cleaved AQP0 (that lacks amino acids 247–263), which is observed in human, bovine, and mouse lens nuclear regions.[22,43,45] The schematic diagram (Figs. 1A, 1B) depicts the strategy used for developing AQP0$^{\Delta C/\Delta C}$ mutant knock-in mouse model (details on the KI mouse model development are given in the Supplementary Section).

Verification of the Absence of CP49 Mutation in the Knockin Mouse Model

KI mice (AQP0$^{+/\Delta C}$ and AQP0$^{\Delta C/\Delta C}$) were genotyped by PCR to verify the absence of the mutation in the beaded filament

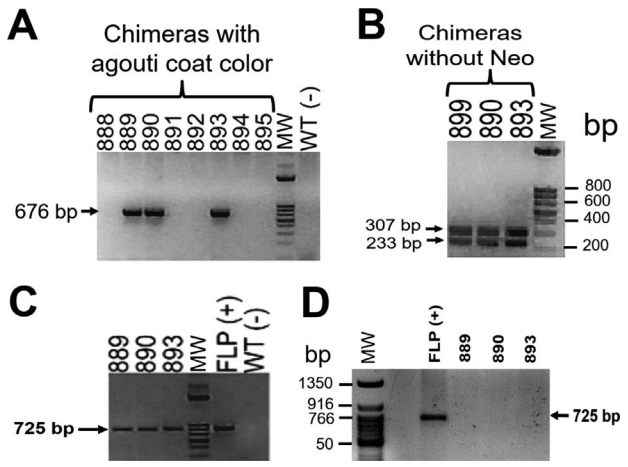

Figure 2. Screening for the introduced stop codon. (**A**) A 676-bp fragment was amplified using revneo3b/MOPE4 primers. MOPE4 is located on the long homology arm (LA, see Fig. 1B), downstream of the deletion. Revneo3b is located inside the Neo cassette. Among the eight agouti-colored chimeras tested, three (#889, 890, and 893) were positive. The PCR product amplified by primers revneo3b and MOPE4 was sequenced to confirm the presence of the introduced stop codon and the fidelity of the amplified fragment. (**B**) Screening for Neo deletion. A primer set Neo deletion primer 1 (NDEL1) and NDEL2 was used to screen mice for the deletion of the Neo cassette. The PCR product for the wild-type is 233 bp. A second band with 307 bp indicates Neo deletion in the chimeras (after Neo deletion, one set of LoxP-FRT sites remain [74 bp] in the KI chimeras). (**C**) Screening for presence of FLP transgene. A primer set, FLP1 and FLP2, used to screen mice for presence of the FLP transgene amplified a positive product of 725 bp; (**D**) FLP-positive and Neo-negative mice were crossed with C57 WT to eliminate FLP transgene. KI mice #889, 890, and 893 were FLP negative with no amplification product while FLP-positive mice genomic DNA amplified 725-bp product. MW, molecular weight marker.

protein *CP49* gene, which was identified originally in mouse 129 strains by Alizadeh et al.[58] Genomic PCR was done using the primers and protocol as described previously.[58,59]

Mass Spectrometric Analysis of Mouse Lens Membrane Protein

Matrix assisted laser desorption/ionization time of flight mass spectrometry (MALDI-TOF MS) analysis was performed at our University Facility as described.[22] The following lenses from WT, $AQP0^{+/\Delta C}$, and $AQP0^{\Delta C/\Delta C}$ at postnatal day 5 (P5) were analyzed (details of the protocol are provided in the Supplementary Section).

Western Blotting

Western blotting was done as described previously.[60] To validate CP49 protein expression, total lens membrane proteins of WT, $AQP0^{+/\Delta C}$, and $AQP0^{\Delta C/\Delta C}$ mice (P5) were prepared and immunoblotting was performed using CP49 antibody.

To verify the expression of AQP0, membrane proteins were extracted from the lenses (at P5) of WT, $AQP0^{+/\Delta C}$, or $AQP0^{\Delta C/\Delta C}$ mouse pups. Mouse monoclonal AQP0 antibody (sc-376445: Santa Cruz Biotechnology, Inc., Dallas, TX, USA) was used (for details, please see the Supplementary Section).

Immunohistochemistry

Lens immunohistochemical studies were conducted as described.[37,60] Lens sections were immunostained using mouse monoclonal AQP0 antibody (Santa Cruz Biotechnology, Inc.) (more information is given in the Supplementary Section).

Evaluation of Lens Transparency and Aberration

Lens transparency was assessed as described by Kumari et al.[37] In brief, lenses of WT, $AQP0^{+/-}$, $AQP0^{-/-}$, $AQP0^{+/\Delta C}$, or $AQP0^{\Delta C/\Delta C}$ mice were dissected out in prewarmed (37°C) mammalian physiological saline. Images of these lenses were captured under the same lighting and imaging conditions with the aid of a dark-field binocular microscope attached to a digital camera. Lens transparency was quantified from the dark field lens images using ImageJ software (http://imagej.nih.gov/ij/; provided in the public domain by the National Institutes of Health, Bethesda, MD, USA). Pixel brightness intensity data were translated into a histogram using SigmaPlot 10 software (Systat Software, Inc., San Jose, CA, USA). Qualitative evaluation of lens aberrations was performed using dark-field optical grid focusing. A copper electron microscope specimen grid was imaged through a whole lens placed on it. Quality of the grid lines focused was appraised for light scatter and aberrations due to refractive index gradient alteration.

Cell Culture and Transfection of AQP0

These procedures were performed basically as described by Varadaraj et al.[27] (details are provided in the Supplementary Section).

Statistical Analysis

SigmaPlot 10 software was used for Student's *t*-tests. P values ≤ 0.05 were considered significant.

Results

Introduction of a stop codon after amino acid 246 in mouse AQP0 was achieved by homologous recombination. Genomic sequencing showed that there was no disruption in the native AQP0 locus (data not shown). To verify the presence of the introduced mutation, genomic DNA from eight mouse chimeras with agouti coat color (#888, 889, 890, 891, 892, 893, 894, and 895) was PCR amplified using primers revneo3b located inside the Neo cassette and MOPE4 located on the long homology arm. Among the eight chimeras tested, #889, 890, and 893 amplified a predicted 676-bp DNA segment (Fig. 2A); the amplicons were sequenced for verification of the introduced stop codon and deletion. To delete the *Neo* gene in the mutant chimeras, #889, 890, and 893 were crossed with FLP transgenic mice. Deletion of the Neo cassette was confirmed by genomic PCR screening of offspring using primer set NDEL1 and NDEL2. Mutant chimeras showed a PCR product of 233 bp for the WT allele and a 307-bp amplicon for the Neo deletion of the mutant allele (Fig. 2B). Presence of the *FLP* gene was confirmed in all three chimeras by PCR, which amplified a 725-bp fragment (Fig. 2C). The three positive mutant chimeras were crossed with C57 WT mice to eliminate FLP transgene; deletion of the FLP transgene was confirmed by genomic PCR (Fig. 2D). The FLP-negative mice were crossed with WT C57 mouse for more than 15 generations before characterizing the phenotype. Interbreeding between heterozygous ($AQP0^{+/\Delta C}$) parents produced offspring in a Mendelian ratio, as determined by PCR analysis (data not shown).

KI mouse pups were genotyped to authenticate the absence of CP49 deletion mutation. WT and KI ($AQP0^{+/\Delta C}$ and $AQP0^{\Delta C/\Delta C}$) mice genomic DNAs amplified a 320-bp PCR

Investigative Ophthalmology & Visual Science

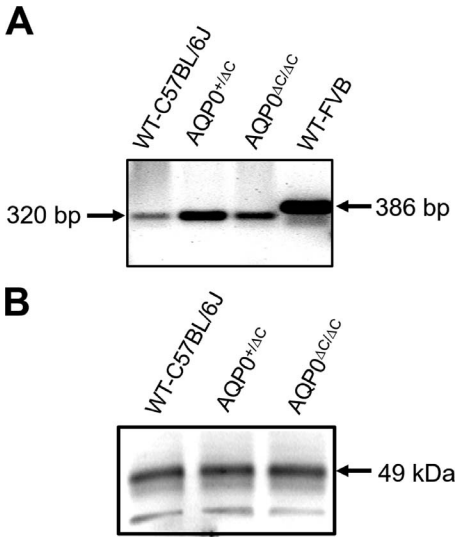

Figure 3. (**A**) Genotyping of C57 WT and KI ($AQP0^{+/\Delta C}$ and $AQP0^{\Delta C/\Delta C}$), and FVB WT mice to show the absence or presence of CP49 natural mutation. An amplicon of 320 bp indicates the presence of intact CP49 allele; 386-bp amplicon indicates the presence of mutant CP49 allele. (**B**) Western blotting of lens proteins of C57 WT and KI mice ($AQP0^{+/\Delta C}$ and $AQP0^{\Delta C/\Delta C}$) to confirm the expression of CP49 protein. Blot treated with CP49 antibody (*arrow* CP49, ~49 kDa).

amplicon indicating the absence of *CP49* gene mutation. The FVB mouse genomic DNA amplified a 386-bp PCR product indicating the presence of the mutant CP49 alleles (Fig. 3A). Immunoblotting of total lens membrane proteins of WT, $AQP0^{+/\Delta C}$, and $AQP0^{\Delta C/\Delta C}$ mice using CP49 antibody verified the expression of CP49 (Fig. 3B).

Protein expression profile of WT, $AQP0^{+/\Delta C}$, or $AQP0^{\Delta C/\Delta C}$ mouse lenses at P5 was characterized by MALDI-TOF MS and Western blotting analyses. Both modes of protein expression analyses showed that WT expressed the 28.2-kDa protein corresponding to intact AQP0, whereas $AQP0^{+/\Delta C}$ expressed 28.2 and 26.5 kDa polypeptides corresponding to intact and cleaved form; $AQP0^{\Delta C/\Delta C}$ lens expressed only the cleaved form of 26.5 kDa (Figs. 4A, 4B). Quantification of the immunoreactive bands representing the intact and cleaved forms in $AQP0^{+/\Delta C}$ mouse lens showed no statistically significant difference ($P > 0.05$) in antibody binding. Immunohistochemical analysis of lenses of P5 sagittal and cross sections of WT and $AQP0^{\Delta C/\Delta C}$ showed fiber cell membrane localization of C-terminal end-cleaved AQP0, very similar to the intact AQP0 expressed in the fiber cell plasma membrane of the WT lens (Fig. 4B); quantification bar graph showed comparable intensity in antibody binding between WT and KI lens cross sections.

After verifying normal trafficking and membrane localization of AQP0 KI protein, we imaged the lenses at different stages, such as embryonic day 18 (E18), P5, P10, P15, and P20 to examine whether there is any phenotypic difference compared with age-matched WT and $AQP0^{-/-}$ lenses. AT E18, lenses of $AQP0^{\Delta C/\Delta C}$ resembled those of the WT, in contrast to $AQP0^{-/-}$ lenses, which showed lens opacity. Representative images are given as Figure 5A (left column). $AQP0^{\Delta C/\Delta C}$ showed normal lens transparency similar to that of WT at P5 also (Fig. 5B, left column). However, at P10 $AQP0^{\Delta C/\Delta C}$ lens began to show opacity at the nuclear region (Fig. 5C, left column) and by P15 the transparency significantly decreased (Fig. 5D, left column). At P20 the lenses of $AQP0^{\Delta C/\Delta C}$ mice exhibited much severe cataract compared with age-matched $AQP0^{-/-}$ lenses (Fig. 5E). Lens transparency was quantified

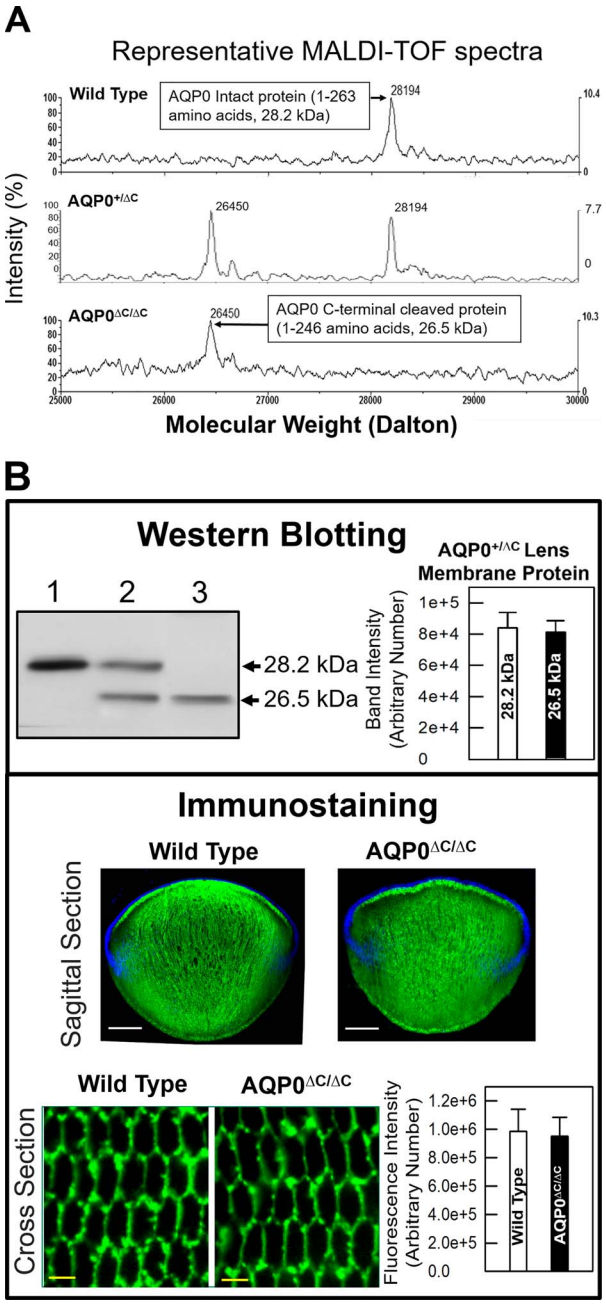

Figure 4. (**A**) Protein expression profile using MALDI/TOF/MS. Lenses of mouse pups at P5 from WT, $AQP0^{+/\Delta C}$, and $AQP0^{\Delta C/\Delta C}$ were used. (**B**) (*Top*) Western blotting of P5 lens proteins of WT (lane 1), $AQP0^{+/\Delta C}$ (lane 2), and $AQP0^{\Delta C/\Delta C}$ (lane 3). The bar graph on the *right* shows quantification of the immunoreactive protein bands of $AQP0^{+/\Delta}$ by densitometry. Values from five independent immunoblots of $AQP0^{+/\Delta C}$ lens membrane proteins were used. Levels of AQP0 C-terminal antibody binding were not significantly ($P > 0.05$) different between the immunoreactive bands of intact AQP0 and C-terminal end-cleaved AQP0. (*Bottom*) Immunostaining. P5 lens sagittal sections of WT and $AQP0^{\Delta C/\Delta C}$ at low magnification. Fluorescent signals in the whole-lens sections appear nonuniform at different areas under low magnification both in the WT and KI lenses due to the thickness of the cryosections, which does not permit uniformity in the imaging plane. *White bar*, 150 μm. Lens cross sections of WT and $AQP0^{\Delta C/\Delta C}$ are shown below at high magnification. Mutant AQP0 protein localized in the fiber cell membranes as in the case of WT lens. *Yellow bar*, 4 μm. The bar graph on the *right* shows quantification of the fluorescence intensity from four independent immunostainings of lens cross sections of WT and $AQP0^{\Delta C/\Delta C}$ mice. Level of fluorescence due to AQP0 C-terminal antibody binding was not significantly different ($P > 0.05$) between WT and $AQP0^{\Delta C/\Delta C}$ lens sections.

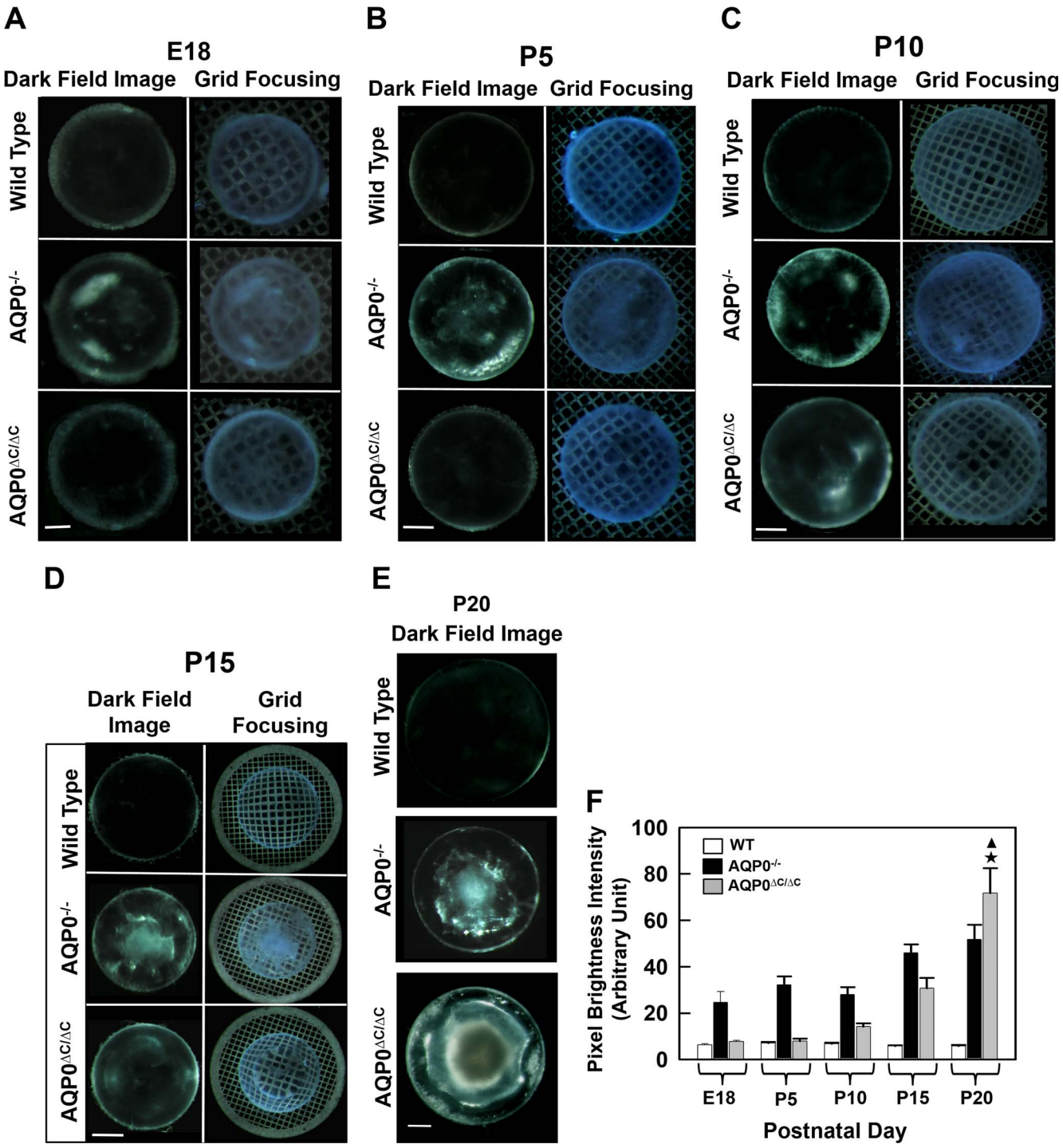

Figure 5. Qualitative characterization of transparency (*left column*) and aberration (*right column*) of WT, AQP0$^{-/-}$, and AQP0$^{\Delta C/\Delta C}$ mouse lenses at (**A**) E18 (*white bar*: 200 µm), (**B**) P5 (*bar*: 320 µm), (**C**) P10 (*bar*: 350 µm), (**D**) P15 (*bar*: 400 µm), and (**E**) P20 (*bar*: 425 µm). (**F**) Quantification of pixel brightness intensity to assess lens transparency in WT, AQP0$^{-/-}$, and AQP0$^{\Delta C/\Delta C}$ mouse lenses at E18, P5, P10, P15, and P20. Higher the pixel brightness intensity, lower would be the lens transparency. *Star* indicates statistical significance, AQP0$^{\Delta C/\Delta C}$ compared with WT at P20 ($P < 0.001$); *filled triangle* indicates statistical significance, AQP0$^{\Delta C/\Delta C}$ compared with AQP0$^{-/-}$ ($P < 0.05$). Note that at P20 lens transparency of AQP0$^{\Delta C/\Delta C}$ lens is much less than that of AQP0$^{-/-}$ lens.

using pixel brightness intensity, which is inversely proportional to transparency (Fig. 5F). Development of lens opacity, which began after P5 in AQP0$^{\Delta C/\Delta C}$ almost doubled with each 5-day postnatal progression in age. By P20, it surpassed the severity of cataract in AQP0$^{-/-}$ lens. The difference in the severity of cataract between the AQP0$^{\Delta C/\Delta C}$ and AQP0$^{-/-}$ lenses was statistically significant. Star in Figure 5F denotes the statistically significant difference compared with the WT lenses ($P < 0.001$) and the triangle indicates significance compared with AQP0$^{-/-}$ ($P < 0.05$).

We tested the lenses for their ability to focus the lines of a copper grid. At E18, the transparent AQP0$^{\Delta C/\Delta C}$ lens focused

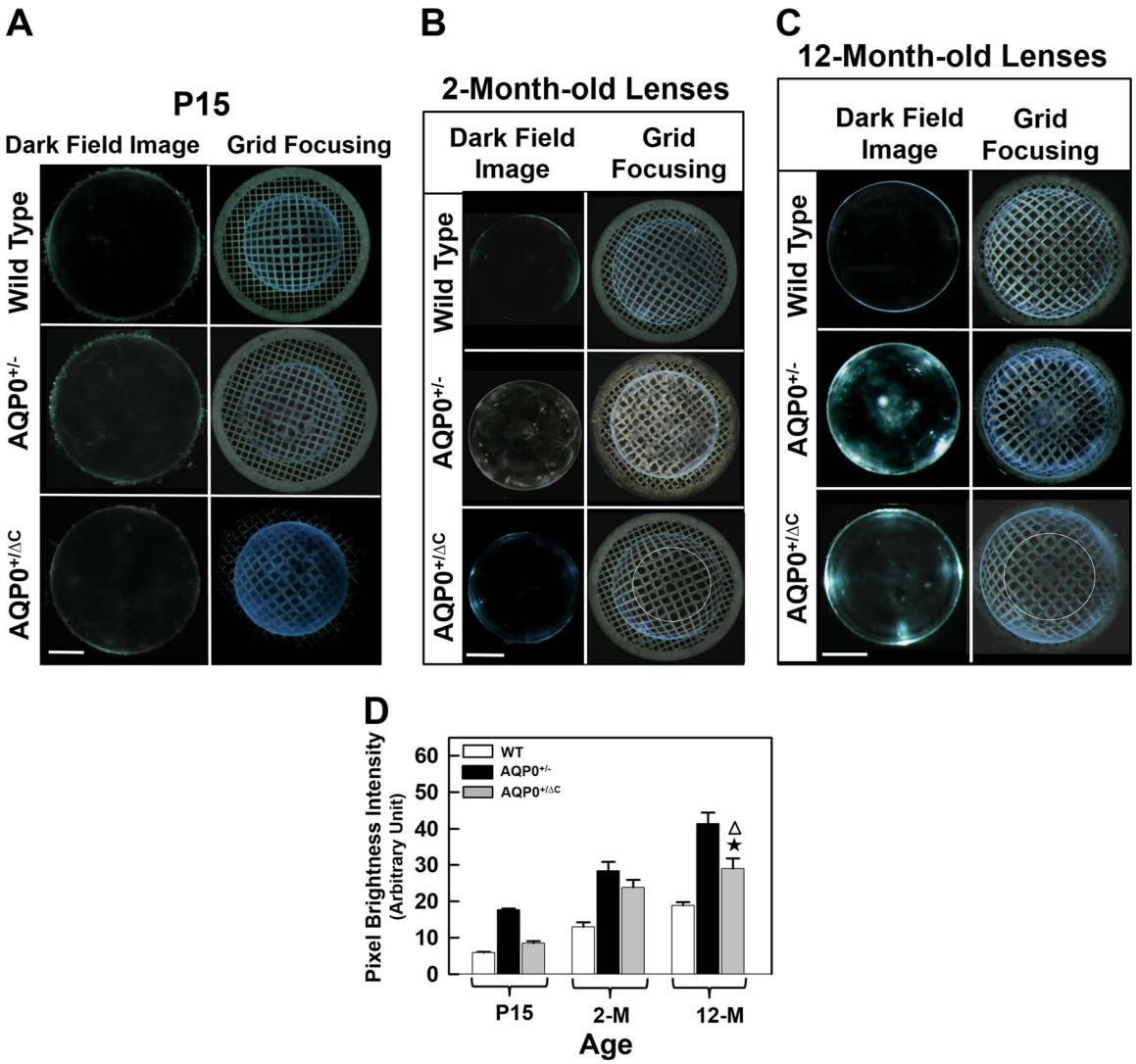

Figure 6. Qualitative characterization of transparency (*left column*) and aberration (*right column*) of WT, AQP0$^{+/-}$, and AQP0$^{+/\Delta C}$ mouse lenses. (**A**) P15 (*white bar*: 400 µm), (**B**) 2-month-old (*bar*: 700 µm; *white circle* denotes the area of aberration), and (**C**) 12-month-old (*bar*: 800 µm; *white circle* denotes the area of aberration). (**D**) Quantification of pixel brightness intensity in WT, AQP0$^{+/-}$, and AQP0$^{+/\Delta C}$ mouse lenses at P15, 2, and 12 months of age. Higher the pixel brightness intensity, lower would be the lens transparency. *Star* indicates statistical significance, AQP0$^{+/\Delta C}$ compared with WT ($P < 0.001$); *open triangle* indicates statistical significance, AQP0$^{+/\Delta C}$ compared with AQP0$^{+/-}$ ($P < 0.05$). Note that lens transparency of AQP0$^{+/\Delta C}$ lens is higher than that of AQP0$^{+/-}$ lens.

the gridlines well like the WT lens and in contrast to the AQP0$^{-/-}$ lens (Fig. 5A, right column). At P5, WT lenses focused copper grid lines sharply (Fig. 5B, right column) and AQP0$^{-/-}$ lenses showed SA due to the cataractous nature of the lens. The AQP0$^{\Delta C/\Delta C}$ lens, which appeared transparent produced distorted grid lines especially at the nuclear region. At P10 and P15, AQP0$^{\Delta C/\Delta C}$ displayed spreading of the central nuclear aberration to the periphery (Figs. 5C, 5D). AQP0$^{-/-}$ lenses showed increase in the severity of SA throughout the lens. By P20 (Fig. 5E), lens cataract was severe in AQP0$^{-/-}$ and AQP0$^{\Delta C/\Delta C}$, notably more in the latter.

The changes we observed in the AQP0$^{\Delta C/\Delta C}$ lenses, prompted us to examine the lenses of AQP0$^{+/\Delta C}$ mice. At early developmental stages, such as P5 and P10, AQP0$^{+/\Delta C}$ lenses with one copy of intact AQP0 did not show lens opacity and aberration like AQP0$^{+/-}$ lenses (data not shown). At P15, dark-field images showed comparable lens transparency (Fig. 6A, left column). However, by P15, both AQP0$^{+/-}$ and AQP0$^{+/\Delta C}$ lenses showed aberration, which was apparent at a much higher degree in the former. AQP0$^{+/\Delta C}$ lenses showed a distinct pattern of central nuclear aberration as revealed by grid focusing (Fig. 6A, right column). Adult 2- (Fig. 6B) and 12-month-old (Fig. 6C) AQP0$^{+/\Delta C}$ lenses showed increased light scattering and central nuclear aberration (red circle), in contrast to global SA in AQP0$^{+/-}$ lens. Figure 6D shows that lens transparency of AQP0$^{+/\Delta C}$ continued to deteriorate with progression in age and the deterioration was statistically significant ($P < 0.05$) compared with the WT at each age shown; however, in AQP0$^{+/\Delta C}$ lens transparency was significantly higher than in AQP0$^{+/-}$.

Optical quality of WT, AQP0$^{+/-}$, AQP0$^{-/-}$, AQP0$^{+/\Delta C}$, and AQP0$^{\Delta C/\Delta C}$ lenses was analyzed from the images of the lenses focusing the electron microscopy grid. The grid line pattern magnified by WT lenses at the tested ages showed a positive barrel distortion aberration (Figs. 5, 6) in which the straight lines bend outward from the image center. The grid line pattern was significantly distorted throughout the lenses in AQP0$^{+/-}$ and AQP0$^{-/-}$. In homozygous KI (AQP0$^{\Delta C/\Delta C}$) lenses,

Investigative Ophthalmology & Visual Science

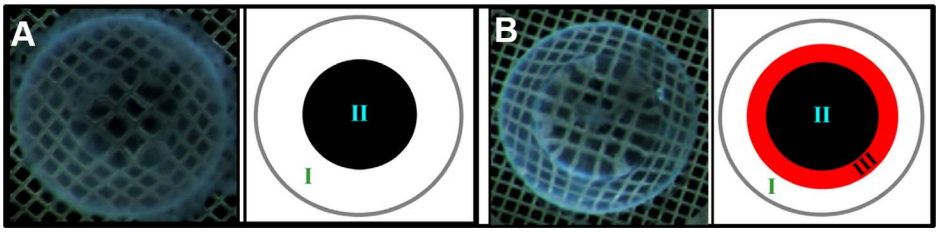

Figure 7. Distortion aberration zones in the lenses of AQP0$^{\Delta C/\Delta C}$ mouse that expresses only C-terminal end-cleaved AQP0. (**A**) An early stage in lens development (P5) showing two distortion aberration zones. (**B**) A later stage (P15) showing three distortion aberration zones.

the much-distorted grid line pattern displayed two distinct zones at P5 (Fig. 5B). Zone I in the cortex showed a barrel distortion aberration (positive radial distortion) as in the WT lenses (Fig. 5B) and Zone II at the lens nucleus showed an abnormally increased barrel distortion aberration compared with WT-lens nucleus. These distortion aberration zones progressively increased in size with the age of the lenses (compare Figs. 5B and 5C). P10 (Fig. 5C) lens exhibited a tendency toward transitioning to a pincushion distortion aberration (negative radial distortion) in the nuclear region. At P15, AQP0$^{\Delta C/\Delta C}$ showed three distinct aberration zones, I, II, and III (Fig. 5D). At this stage, the nuclear Zone II clearly exhibited a pincushion distortion aberration and a new Zone III was established between the Zones I and II (i.e., at the corticonuclear junction) with a greater barrel distortion aberration than that of cortical Zone I. In the heterozygous (AQP0$^{+/\Delta C}$) lenses, only two distortion aberration zones start to appear at age P15 (Fig. 6A), as in the case of AQP0$^{\Delta C/\Delta C}$ lenses at P5 (Fig.5B). These distortion aberration zones slowly progressed with the age of the lens (compare Figs. 6A–C). While P15 (Fig. 6A) lens showed more of a barrel distortion, the 2-month-old lens clearly showed a pincushion distortion (Fig. 6B). There was no distinct Zone III in AQP0$^{+/\Delta C}$ mouse lenses (Fig. 6C). The distortion aberration zones are shown as a schematic model (Fig. 7).

To find out whether the end-cleavage process is part of lens development or a consequence of senescence, we performed Western blotting of membrane proteins extracted from lens fiber cells of P10 pups and adult WT mice. Membrane proteins extracted from AQP0-transfected MDCK cells served as negative control for posttranslationally end-cleaved AQP0. As anticipated, protein samples from MDCK cells exhibited a specific band of 28.2 kDa for expression of the transfected AQP0 indicating the absence of posttranslational truncation. Membrane proteins from mouse lenses at P10 showed two immunoreactive bands of 28.2 and 25.6 kDa. Adult lens membrane proteins showed multiple polypeptides binding to AQP0 antibody including the two peptide bands of 28.2 and 25.6 kDa, as observed for P10 lenses (Fig. 8). These results demonstrate that end-truncation begins at a very early age in life and is not a senescence-dependent phenomenon.

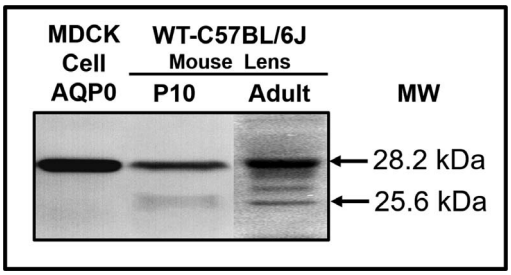

Figure 8. Western blot analysis. Membrane proteins extracted from MDCK cells transfected with mouse intact AQP0 or from the lenses of P10 and 4-month-old adult C57 WT mice were tested. AQP0 C-terminal-specific antibody was used. The C-terminal antibody was raised using an epitope peptide having amino acids 220 to 263. Of note, here, the KI-truncated AQP0 has amino acids up to 246 at the C-terminus.

Discussion

Starting from the outer cortex and leading into the inner nucleus, lens has an array of gradients. Along this gradient, the intracellular pH reads 7.2 to 6.8,[61,62] Ca^{2+} from 300 to 700 nM,[63] protein gradient (less to more), water gradient (more to less) membrane proteins like AQP0, and cytosolic proteins like crystallins as intact soluble (more to less), N- and/or C-terminal end-cleaved insoluble forms (less to more), and refractive index gradient (RING: 1.386–1.406 in human).[4,5] In accordance with this gradient trend, N- and/or C-terminal ends of AQP0, connexin, and crystallin proteins are progressively cleaved toward the center of the lens and remain there throughout life. The purpose behind these events remained puzzling. In a previous study using an AQP0$^{-/-}$ and a transgenic model that expresses AQP1 in the fiber cells of AQP0$^{-/-}$ mouse (TgAQP1$^{+/+}$/AQP0$^{-/-}$), we hypothesized that intact and end-cleaved AQP0 must be playing a crucial role in adjusting the lens RING.[22] The current study corroborates that by demonstrating distortion aberration in the lenses of the AQP0$^{\Delta C/\Delta C}$ mouse model that expresses only cleaved AQP0. Arrangement of intact and cleaved forms in a gradient from the outer cortex to the inner nucleus must be the norm to ensure sharp focusing.

AQP0 is essential for embryonic and postnatal development. This is highlighted in AQP0$^{-/-}$ lens in which loss of lens transparency is fast and severe starting from the early developmental stages (Fig. 5). However, in AQP0$^{\Delta C/\Delta C}$, lens cataract development is either absent or slow in the initial developmental stages but is accelerated in the postnatal stages (Fig. 5E); absence of intact AQP0 during these stages, results in cataract that is more severe than in AQP0$^{-/-}$, suggesting that presence of C-terminal end-cleaved AQP0 in the absence of the intact form could alter lens homeostasis significantly. It can be speculated that alterations in the expression level of intact AQP0 in the differentiating cortical fiber cells and abnormal accelerated N- and C-terminal end-cleavage during senescence could cause lens opacity and cataract due to the loss of homeostasis.

E18 lens showed severe cataract in AQP0$^{-/-}$ whereas the age-matched AQP0$^{\Delta C/\Delta C}$ lens was transparent without any aberrations (Fig. 5A). In the AQP0$^{\Delta C/\Delta C}$ mouse lens there was gradual development of distortion aberration until P15 followed by cataractogenesis (Figs. 5, 6). Absence of intact AQP0 does not appear to affect lens homeostasis significantly during early developmental stages in the AQP0$^{\Delta C/\Delta C}$ lens but is essential during the later stages of postnatal lens development and for transparency. A notable result is the presence of distortion aberration in early postnatal lenses, such as in P5,

even though there was no cataract. Because distortion aberration is a manifestation of alterations in the RING, it can be inferred that albeit the AQP0$^{\Delta C/\Delta C}$ lens manages to be transparent and prolong cataractogenesis, starting at an early age it is unable to establish and maintain the proper RING necessary to avoid distortion aberration. Our data show that in the cortex, presence of the 17 amino acids at the C-terminal end of AQP0 is essential for RING development to ensure transparency and sharp focusing of the lens.

In AQP0$^{+/-}$ mouse lens, presence of 50% of intact and cleaved forms caused loss of transparency, increased SA, and cataract. Presence of 100% of the cleaved forms (as in a WT lens) and 50% intact AQP0 in the AQP0$^{+/\Delta C}$ prolonged the onset of cataract. However, absence of intact AQP0 in the ratio as is present in the WT, did create distortion aberration at P15. AQP0$^{\Delta C/\Delta C}$ developed three distinct distortion (aberration) zones. This could be due to the loss of the arrangement of intact AQP0 and posttranslationally end-cleaved forms in a specific manner from the cortex (more intact AQP0 and less cleaved-AQP0) to the nucleus (less intact AQP0 and more cleaved-AQP0), which is required for lens RING development.[2] Recent studies on a connexin 46 (Cx46) mutant mouse model (Cx46fs380) showed a barrel distortion and a pincushion distortion in the lenses.[64] The phenotypic difference in distortion aberration between AQP0$^{\Delta C/\Delta C}$ and Cx46fs380 mouse models could be due to the functional difference of these proteins in the fiber cell membrane. Also, the mutant Cx46 did not traffic to the membrane[65] whereas the C-terminal end-cleaved AQP0 trafficked to the plasma membrane (Fig. 4B). Our results show that intact and cleaved forms of AQP0 in the appropriate ratio in the lens is essential for the establishment and maintenance of RING, transparency, and homeostasis.

The lens grows continuously. Normal end-cleavage of AQP0 is not aging-related (senescence-related) but it is associated with fiber cell maturation process to adjust the lens RING. For example, in early-postnatal young lenses, such as in P10, differentiating fiber cells are more and contain only intact AQP0, the number of which is more than that in the mature fiber cells that carry both intact and cleaved AQP0. The opposite is true in the adult lenses. P10 lenses have less end-cleaved AQP0 due to the small volume of mature fiber cells than adult lenses that contain a large volume of mature fiber cells and more end-cleaved AQP0. The difference in the ratios of intact versus cleaved AQP0 between young and adult is not due to aging but due to the amount of differentiating and mature fiber cells in the lens. Mature adult contains more mature fiber cells in the inner cortex and nucleus and therefore the volume of cleaved forms is more. The 17 amino acid C-terminal end-cleaved AQP0 also showed a similar trend in human lens[43]; however, there was senescence-related abnormally accelerated rate of C-terminal end-cleavage in AQP0. The study by Korlimbinis et al.[43] on human lens AQP0 shows that normal C-terminal end-cleavage is a part of the fiber cell maturation process and an increase in intact versus cleaved forms is mainly due to the size of the lens; second, the aging process could induce abnormally accelerated end-cleavage and lead to aging-related blurred vision.

With its virtues of low water permeability,[10–15,66] high CTCA property[2,15–21,32–34,67,68] and capability of undergoing end-cleavage,[2,22,43,45] AQP0 could play a major role in the formation and maintenance of RING.[2] Intact AQP0 forms small patches of square array thin junctions in the cortex and cleaved forms facilitate formation of large patches of thin junctions in the nuclear region,[67] potentially to regulate fiber cell adhesion efficiency.[34,68] The C-terminal ends of intact AQP0 at the outer cortex interact with other proteins, such as beaded filament proteins filensin and CP49, to provide anchorage, fiber cell architecture, and lens biomechanics. Interaction of adhesion protein N-Cadherin and cytoskeletal elements during fiber cell elongation has been reported.[69] CTCA is necessary to maintain the proper RING, which is low at the outer cortex and high in the central nucleus where it is more or less constant.[70,71] Absence of C-terminal end of AQP0 in the KI lens could be facilitating the formation of large patches of thin junctions globally in the lens and such increased CTCA of unfavorable measures at the outer cortex could be correspondingly altering the refractive index at this region. Our data suggest that presence of intact AQP0 is a necessity to establish the RING conducive for proper focusing. To adjust the refractive index, end-cleavage should occur gradually, starting from the inner cortex, concomitant with dehydration of the fiber cells. Slow and steady processes like these within the fiber cells confer optical and biomechanical properties suitable for focusing light from objects near or far.

In conclusion, a conducive ratio of intact and C-terminal end-cleaved forms of AQP0 must be maintained in a spatial and temporal distribution manner to maintain lens transparency, RING and homeostasis in the continually growing lens for precise focusing. Until the questions of how the end-cleavages occur in the lens and what are the mechanisms involved are deciphered, developing a reciprocal mouse model with only intact AQP0 in the lens would remain a far-fetched goal.

Acknowledgments

The authors thank Alan Shiels (Washington University, St. Louis, MO, USA) for providing AQP0 knockout mixed strain mouse and to Paul FitzGerald (University of California, Davis, CA, USA) for providing CP49 antibody.

Supported by National Institutes of Health-National Eye Institute R01 Grant EY026155.

Disclosure: **K. Varadaraj**, None; **S. Kumari**, None

References

1. Pierscionek BK, Regini JW. The gradient index lens of the eye: an opto-biological synchrony. *Prog Retin Eye Res*. 2012;31:332–349.
2. Kumari SS, Varadaraj K. Intact and N- or C-terminal end truncated AQP0 function as open water channels and cell-to-cell adhesion proteins: end truncation could be a prelude for adjusting the refractive index of the lens to prevent spherical aberration. *Biochim Biophys Acta*. 2014;1840:2862–2877.
3. Hecht E. *Optics*. 2nd ed. Boston: Addison Wesley; 1987.
4. Garner LF, Ooi CS, Smith G. Refractive index of the crystalline lens in young and aged eyes. *Clin Exp Optom*. 1998;81:145–150.
5. Hoshino M, Uesugi K, Yagi N, Mohri S, Regini J, Pierscionek B. Optical properties of in situ eye lenses measured with X-ray Talbot interferometry: a novel measure of growth processes. *PLoS One*. 2011;6:e25140.
6. Mathias RT, Rae JL, Baldo GJ. Physiological properties of the normal lens. *Physiol Rev*. 1997;77:21–50.
7. Mathias RT, Kistler J, Donaldson P. The lens circulation. *J Membr Biol*. 2007;216:1–16.
8. Gao J, Sun X, White TW, Delamere NA, Mathias RT. Feedback regulation of intracellular hydrostatic pressure in surface cells of the lens. *Biophys J*. 2015;109:1830–1839.
9. Bassnett S, Wilmarth PA, David LL. The membrane proteome of the mouse lens fiber cell. *Mol Vis*. 2009;15:2448–2463.
10. Mulders SM, Preston GM, Deen PM, Guggino WB, van Os CH, Agre P. Water channel properties of major intrinsic protein of lens. *J Biol Chem*. 1995;270:9010–9016.

11. Varadaraj K, Kushmerick C, Baldo GJ, et al. The role of MIP in lens fiber cell membrane transport. *J Membr Biol*. 1999;170: 191–203.
12. Shiels A, Bassnett S, Varadaraj K, et al. Optical dysfunction of the crystalline lens in aquaporin-0-deficient mice. *Physiol Genomics*. 2001;7:179–186.
13. Kushmerick C, Rice SJ, Baldo GJ, Haspel HC, Mathias RT. Ion, water and neutral solute transport in *Xenopus* oocytes expressing frog lens MIP. *Exp Eye Res*. 1995;61:351–362.
14. Zampighi GA, Kreman M, Boorer KJ, et al. A method for determining the unitary functional capacity of cloned channels and transporters expressed in Xenopus laevis oocytes. *J Membr Biol*. 1995;148:65–78.
15. Varadaraj K, Kumari S, Mathias T. Transgenic expression of AQP1 in the fiber cells of AQP0 knockout mouse: effects on lens transparency. *Exp Eye Res*. 2010;91:393–404.
16. Kumari SS, Eswaramoorthy S, Mathias RT, Varadaraj K. Unique and analogous functions of aquaporin 0 for fiber cell architecture and ocular lens transparency. *Biochim Biophys Acta*. 2011;1812:1089–1097.
17. Liu J, Xu J, Gu S, Nicholson BJ, Jiang JX. Aquaporin 0 enhances gap junction coupling via its cell adhesion function and interaction with connexin 50. *J Cell Sci*. 2011;124:198–206.
18. Michea LF, de la Fuente M, Lagos N. Lens major intrinsic protein (MIP) promotes adhesion when reconstituted into large unilamellar liposomes. *Biochemistry*. 1994;33:7663–7669.
19. Michea LF, Andrinolo D, Ceppi H, Lagos N. Biochemical evidence for adhesion-promoting role of major intrinsic protein isolated from both normal and cataractous human lenses. *Exp Eye Res*. 1995;61:293–301.
20. Kumari SS, Varadaraj K. Intact AQP0 performs cell-to-cell adhesion. *Biochem Biophys Res Commun*. 2009;390:1034–1039.
21. Lo WK, Biswas SK, Brako L, Shiels A, Gu S, Jiang JX. Aquaporin-targets interlocking domains to control the integrity and transparency of the eye lens. *Invest Ophthalmol Vis Sci*. 2014;55:1202–1212.
22. Kumari SS, Varadaraj K. Aquaporin 0 plays a pivotal role in refractive index gradient development in mammalian eye lens to prevent spherical aberration. *Biochem Biophys Res Commun*. 2014;445:986–991.
23. Kumari SS, Gupta N, Shiels A, et al. Role of Aquaporin 0 in lens biomechanics. *Biochem Biophys Res Commun*. 2015; 462:339–345.
24. Hall JE, Mathias RT. The aquaporin zero puzzle. *Biophys J*. 2014;107:10–15.
25. Ruiz-Ederra J, Verkman AS. Accelerated cataract formation and reduced lens epithelial water permeability in aquaporin-1-deficient mice. *Invest Ophthalmol Vis Sci*. 2006;47:3960–3967.
26. Kumari S, Varadaraj K. Aquaporin 5 knockout mouse lens develops hyperglycemic cataract. *Biochem Biophys Res Commun*. 2013;441:333–338.
27. Varadaraj K, Kumari SS, Patil R, Wax MB, Mathias RT. Functional characterization of a human aquaporin 0 mutation that leads to a congenital dominant lens cataract. *Exp Eye Res*. 2008;87:9–21.
28. Kumari SS, Gandhi J, Mustehsan MH, Eren S, Varadaraj K. Functional characterization of an AQP0 missense mutation, R33C, that causes dominant congenital lens cataract, reveals impaired cell-to-cell adhesion. *Exp Eye Res*. 2013;116:371–385.
29. Schey KL, Wang Z, Wenke JL, Qi Y. Aquaporins in the eye: expression, function, and roles in ocular disease. *Biochim Biophys Acta*. 2014;1840:1513–1523.
30. Zhou Y, Bennett TM, Shiels A. Lens ER-stress response during cataract development in Mip-mutant mice. *Biochim Biophys Acta*. 2016;1862:1433–1442.
31. Buzhynskyy N, Girmens JF, Faigle W, Scheuring S. Human cataract lens membrane at subnanometer resolution. *J Mol Biol*. 2007;374:162–169.
32. Buzhynskyy N, Sens P, Behar-Cohen F, Scheuring S. Eye lens membrane junctional microdomains: a comparison between healthy and pathological cases. *New J Phys*. 2011;13:085016.
33. Mangenot S, Buzhynskyy N, Girmens JF, Scheuring S. Malformation of junctional microdomains in cataract lens membranes from a type II diabetes patient. *Pflugers Arch*. 2009;457:1265–1274.
34. Vorontsova I, Gehring I, Hall JE, Schilling TF. Aqp0a regulates suture stability in the zebrafish lens. *Invest Ophthalmol Vis Sci*. 2018;59:2869–2879.
35. Németh-Cahalan KL, Clemens DM, Hall JE. Regulation of AQP0 water permeability is enhanced by cooperativity. *J Gen Physiol*. 2013;141:287–295.
36. Fields JB, Németh-Cahalan KL, Freites JA, Vorontsova I, Hall JE, Tobias DJ. Calmodulin gates Aquaporin 0 permeability through a positively charged cytoplasmic loop. *J Biol Chem*. 2017;292:185–195.
37. Kumari S, Gao J, Mathias RT, et al. Aquaporin 0 modulates lens gap junctions in the presence of lens-specific beaded filament proteins. *Invest Ophthalmol Vis Sci*. 2017;58:6006–6019.
38. Lindsey Rose KM, Gourdie RG, Prescott AR, Quinlan RA, Crouch RK, Schey KL. The C terminus of lens aquaporin 0 interacts with the cytoskeletal proteins filensin and CP49. *Invest Ophthalmol Vis Sci*. 2006;47:1562–1570.
39. Wang Z, Schey KL. Identification of a direct Aquaporin-0 binding site in the lens-specific cytoskeletal protein filensin. *Exp Eye Res*. 2017;159:23–29.
40. Schey KL, Petrova RS, Gletten RB, Donaldson PJ. The role of Aquaporins in ocular lens homeostasis. *Int J Mol Sci*. 2017;18: E2693.
41. Roy D, Spector A, Farnsworth PN. Human lens membrane: comparison of major intrinsic polypeptides from young and old lenses isolated by a new methodology. *Exp Eye Res*. 1979; 28:353–358.
42. Schey KL, Little M, Fowler JG, Crouch RK. Characterization of human lens major intrinsic protein structure. *Invest Ophthalmol Vis Sci*. 2000;41:175–182.
43. Korlimbinis A, Berry Y, Thibault D, Schey KL, Truscott RJ. Protein aging: truncation of aquaporin 0 in human lens regions is a continuous age-dependent process. *Exp Eye Res*. 2009;88:966–973.
44. Ball LE, Wang Z, Schey KL. Identification of a direct Aquaporin-0 binding site in the lens-specific cytoskeletal protein filensin. *Exp Eye Res*. 2017;159:23–29.
45. Ball LE, Garland DL, Crouch RK, Schey KL. Post-translational modifications of aquaporin 0 (AQP0) in the normal human lens: spatial and temporal occurrence. *Biochemistry*. 2004; 43:9856–9865.
46. Takemoto LJ. Quantitation of specific cleavage sites at the C-terminal region of alpha-A crystallin from human lenses of different age. *Exp Eye Res*. 1998;66:263–266.
47. Lund AL, Smith JB, Smith DL. Modifications of the water-insoluble human lens alpha-crystallins. *Exp Eye Res*. 1996;63: 661–672.
48. Kistler J, Bullivant S. Protein processing in lens intercellular junctions: cleavage of MP70 to MP38. *Invest Ophthalmol Vis Sci*. 1987;28:1687–1692.
49. Lin JS, Fitzgerald S, Dong YM, Knight C, Donaldson P, Kistler J. Processing of the gap junction protein connexin50 in the ocular lens is accomplished by calpain. *Eur J Cell Biol*. 1997; 73:141–149.
50. Lin JS, Eckert R, Kistler J, Donaldson P. Spatial differences in gap junction gating in the lens are a consequence of connexin cleavage. *Eur J Cell Biol*. 1998;76:246–250.

Investigative Ophthalmology & Visual Science

51. Xu X, Berthoud VM, Beyer EC, Ebihara L. Functional role of the carboxyl terminal domain of human connexin 50 in gap junctional channels. *J Membr Biol*. 2002;186:101–112.
52. Tenbroek E, Arenson M, Jarvis L, Loius C. The distribution of the fiber cell intrinsic membrane proteins MP20 and connexin46 in the bovine lens. *J Cell Sci*. 1992;103:245–257.
53. Jacobs MD, Soeller C, Sisley AM, Cannell MB, Donaldson PJ. Gap junction processing and redistribution revealed by quantitative optical measurements of connexin46 epitopes in the lens. *Invest Ophthalmol Vis Sci*. 2004;45:191–199.
54. FitzGerald PG. Age-related changes in a fiber cell-specific extrinsic membrane protein. *Curr Eye Res*. 1988;7:1255–1262.
55. Wang Z, Obidike JE, Schey KL. Posttranslational modifications of the bovine lens beaded filament proteins filensin and CP49. *Invest Ophthalmol Vis Sci*. 2010;51:1565–1574.
56. Do Ngoc L, Paroutaud P, Dunia I, Benedetti EL, Hoebeke J. Sequence analysis of peptide fragments from the intrinsic membrane protein of calf lens fibers MP26 and its natural maturation product MP22. *FEBS Lett*. 1985;181:74–78.
57. Schey KL, Fowler JG, Shearer TR, David LL. Modifications to rat lens major intrinsic protein in selenite-induced cataract. *Invest Ophthalmol Vis Sci*. 1999;40:657–667.
58. Alizadeh A, Clark J, Seeberger T, Hess J, Blankenship T, FitzGerald PG. Characterization of a mutation in the lens-specific CP49 in the 129 strain of mouse. *Invest Ophthalmol Vis Sci*. 2004;45:884–891.
59. Simirskii VN, Lee RS, Wawrousek EF, Duncan MK. Inbred FVB/N mice are mutant at the cp49/Bfsp2 locus and lack beaded filament proteins in the lens. *Invest Ophthalmol Vis Sci*. 2006;47:4931–4934.
60. Varadaraj K, Kumari SS, Mathias RT. Functional expression of aquaporins in embryonic, postnatal, and adult mouse lenses. *Dev Dyn*. 2007;236:1319–1328.
61. Mathias RT, Riquelme G, Rae JL. Cell to cell communication and pH in the frog lens. *J Gen Physiol*. 1991;98:1085–1103.
62. Bassnett S, Croghan PC, Duncan G. Diffusion of lactate and its role in determining intracellular pH in the lens of the eye. *Exp Eye Res*. 1987;44:143–147.
63. Gao J, Sun X, Martinez-Wittinghan FJ, Gong X, White TW, Mathias RT. Connections between connexins, calcium, and cataracts in the lens. *J Gen Physiol*. 2004;124:289–300.
64. Minogue PJ, Gao J, Zoltoski RK, et al. Physiological and optical alterations precede the appearance of cataracts in Cx46fs380 mice. *Invest Ophthalmol Vis Sci*. 2017;58:4366–4374.
65. Minogue PJ, Liu X, Ebihara L, Beyer EC, Berthoud VM. An aberrant sequence in a connexin46 mutant underlies congenital cataracts. *J Biol Chem*. 2005;280:40788–40795.
66. Chandy G, Zampighi GA, Kreman M, Hall JE. Comparison of the water transporting properties of MIP and AQP1. *J Membr Biol*. 1997;159:29–39.
67. Zampighi GA, Eskandari S, Hall JE, Zampighi L, Kreman M. Micro-domains of AQP0 in lens equatorial fibers. *Exp Eye Res*. 2002;75:505–519.
68. Varadaraj K, Kumari SS. Molecular mechanism of Aquaporin 0-induced fiber cell to fiber cell adhesion in the eye lens. *Biochem Biophys Res Commun*. 2018;506:284–289.
69. Logan CM, Bowen CJ, Menko AS. Functional role for stable microtubules in lens fiber cell elongation. *Exp Cell Res*. 2018;362:477–488.
70. Jones CE, Atchison DA, Meder R, Pope JM. Refractive index distribution and optical properties of the isolated human lens measured using magnetic resonance imaging (MRI). *Vision Res*. 2005;45:2352–2366.
71. Uhlhorn SR, Borja D, Manns F, Parel JM. Refractive index measurement of the isolated crystalline lens using optical coherence tomography. *Vision Res*. 2008;48:2732–2738.

Investigative Ophthalmology & Visual Science